Chapter 3

PRODUCTION AND FATE OF C_4 DIHYDROXYCARBONYL COMPOUNDS FROM ISOPRENE OXIDATION

Bates, K. H., T. B. Nguyen, A. P. Teng, J. D. Crounse, H. G. Kjaergaard, B. M. Stoltz, J. H. Seinfeld, and P. O. Wennberg (2016). "Production and fate of C4 dihydroxycarbonyl compounds from isoprene oxidation". In: *J. Phys. Chem. A* 120.1, pp. 106–117. DOI: 10.1021/acs.jpca.5b10335.

Abstract

isoprene epoxydiols (IEPOX) are formed in high yield as second-generation products of atmospheric isoprene oxidation in pristine (low-NO) environments. IEPOX has received significant attention for its ability to form secondary organic aerosol, but the fate of IEPOX in the gas phase, and those of its oxidation products, remains largely unexplored. In this study, three dihydroxycarbonyl compounds with molecular formula of $C_4H_8O_3$ – putative products of IEPOX oxidation – are synthesized to determine their isomer-specific yields from IEPOX. We find that 3,4-dihydroxy-2-butanone (DHBO) comprises 43% and 36% of the products from *cis*- and *trans*-β-IEPOX respectively, and is by far the most abundant $C_4H_8O_3$ dihydroxycarbonyl compound produced by this mechanism. OH is found to react with DHBO with a rate coefficient of 1.10×10^{-11} cm^3 molecule^{-1} s^{-1} at 297 K, forming two hydroxydicarbonyl compounds that share the molecular formula $C_4H_6O_3$ with unitary yield. The results of this study are compared with field observations and used to propose a multigenerational mechanism of IEPOX oxidation. Finally, global simulations using GEOS-Chem, a chemical transport model, show that the $C_4H_8O_3$ dihydroxycarbonyl compounds and their oxidation products are widespread in the atmosphere, and estimate annual global production of $C_4H_8O_3$ dihydroxycarbonyls to be 54 Tg y^{-1}, primarily as DHBO.

3.1 Introduction

Atmospheric emissions of isoprene, derived primarily from deciduous plants, are estimated to exceed 500 Tg y^{-1} globally, making isoprene the most abundantly emitted non-methane hydrocarbon by mass (Guenther *et al.*, 2006; Guenther *et al.*, 2012). The rapid oxidation of both isoprene and its oxidation products in

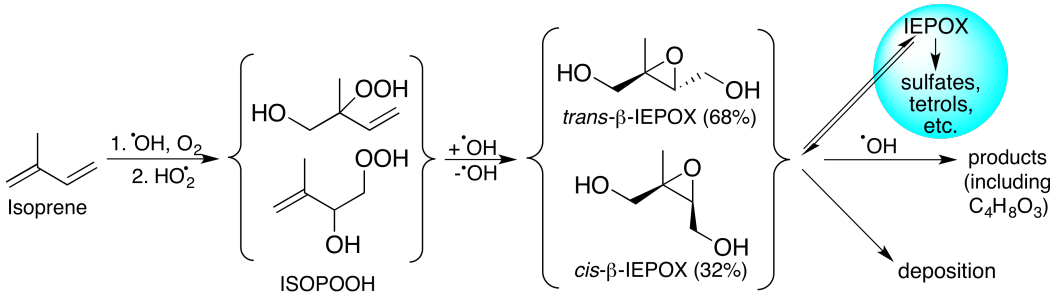

Figure 3.1: Steps and compounds in the HO_x-mediated (low-NO) oxidation of isoprene.

the gas phase, principally by OH radicals (Atkinson *et al.*, 2006), helps to set the atmosphere's oxidative capacity and leads to the formation of both highly oxygenated gaseous compounds and secondary organic aerosol (SOA) (Archibald *et al.*, 2010; Lelieveld *et al.*, 2008). These effects can exert a strong influence on climate, health, and tropospheric chemistry in areas with high biogenic emissions.

In regions of the atmosphere with low concentrations of NO, which typically occur in remote forests where isoprene emissions are high, the oxidation of isoprene proceeds predominantly by a HO_x-mediated (OH + HO_2) pathway shown in Figure 3.1 (Kuhlmann and Lawrence, 2004; Rosenstiel *et al.*, 2003; Wiedinmyer *et al.*, 2006). The addition of OH and O_2 is followed by reaction with HO_2 to form hydroxy hydroperoxides (ISOPOOH) in yields of >80% (Crutzen *et al.*, 2000; Paulot *et al.*, 2009b). A recent synthetic route to the dominant ISOPOOH isomers has facilitated measurements of the rates and products of their reactions with OH (St. Clair *et al.*, 2015), which previously relied on estimates from OH + isoprene experiments (Paulot *et al.*, 2009b). The dominant fate of ISOPOOH is reaction with OH to form isoprene epoxydiols (IEPOX) in yields of 70-80%, resulting in an isomeric ratio of 2:1 for *trans-* to *cis-β*-IEPOX (St. Clair *et al.*, 2015). This reaction recycles one equivalent of OH (Paulot *et al.*, 2009b), contributing to the stability of HO_x in remote forested regions (Lelieveld *et al.*, 2008; Ren *et al.*, 2008; Thornton *et al.*, 2002).

In the atmosphere, IEPOX can then follow a number of subsequent pathways. IEPOX has been shown to contribute substantially to biogenic SOA in the field (Budisulistiorini *et al.*, 2013; Froyd *et al.*, 2011; Worton *et al.*, 2013; Zhang *et al.*, 2013), where its aerosol uptake depends on a variety of factors such as particle liquid water content, total particulate surface area, anionic activity (*e.g.* sulfate

and other nucleophiles), cationic activity (primarily hydronium in many areas), and organic coating (Gaston *et al.*, 2014; Liao *et al.*, 2015; Nguyen *et al.*, 2014a; Surratt *et al.*, 2010; Xu *et al.*, 2015). The properties of its reactive uptake have been further examined in chamber experiments (Gaston *et al.*, 2014; Lin *et al.*, 2012; Liu *et al.*, 2015; Nguyen *et al.*, 2014a; Surratt *et al.*, 2010), facilitated by the development of synthetic routes to four IEPOX isomers (Zhang *et al.*, 2012). A laboratory study focusing on particle free acidity and surface area placed constraints on IEPOX aerosol uptake at <5 h (pH <1) to >25 h (pH >3), and noted that organic coatings on aerosols significantly suppress IEPOX uptake, suggesting that the aerosol uptake can be self-limiting (Gaston *et al.*, 2014). These results imply that particle uptake may be the dominant IEPOX loss process only when aerosol pH is less than 1 on freshly exposed aqueous sulfate particles.

Additional IEPOX loss processes include deposition and reaction with OH in the gas phase. Dry deposition of IEPOX and its gas phase oxidation products to a forested environment has also been measured in the field, with a typical lifetime of 13 h under daytime turbulent mixing conditions (Nguyen *et al.*, 2015a). Laboratory studies of the gas phase oxidation of IEPOX by OH measured lifetimes of 3-28 h, and identified a number of stable products (Bates *et al.*, 2014; Jacobs *et al.*, 2013). All together, previous work suggests that gas phase reaction with OH dominates IEPOX loss (~44%) under environmental conditions typical of IEPOX production (daytime, turbulent 1.5 km mixed layer, ~200 μm^2 cm^{-3} particle surface area with aerosol pH = 3), with deposition (~37%) and particle uptake (~19%) contributing smaller proportions (Bates *et al.*, 2014; Gaston *et al.*, 2014; Nguyen *et al.*, 2015a).

Bates *et al.* (2014) identified a dominant product from the gas phase oxidation of both the *cis*- and *trans*-β-IEPOX by OH as an unknown compound with a nominal mass of 104 a.m.u., with yields of 33 (±11) %. A likely formula of $C_4H_8O_3$ was assigned to the product, and two possible structures were proposed, but no further information on the compound(s) could be determined. Given the high measured yields and the atmospheric importance of IEPOX – with an estimated 226 Tg y^{-1} produced globally (St. Clair *et al.*, 2015) – the identity and subsequent fate of this unknown product may have profound impacts on oxidant budgets, SOA formation, and other important aspects of tropospheric chemistry in low-NO high-isoprene environments.

In the experiments detailed here, standards of IEPOX and three $C_4H_8O_3$ compounds, shown in Figure 3.2, were synthesized in order to identify these 104 a.m.u.

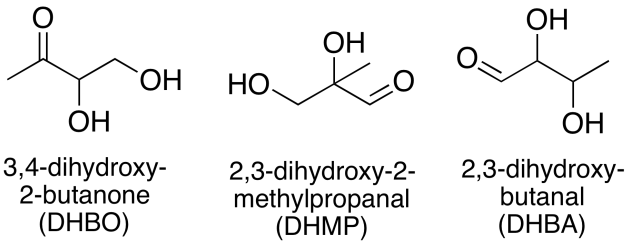

Figure 3.2: Dihydroxycarbonyl species synthesized and investigated in this study, collectively referred to as $C_4H_8O_3$.

products of IEPOX + OH and to measure their yields with greater precision, using an improved gas chromatography-chemical ionization mass spectrometry (GC-CIMS) technique. The rates and products of the reactions of the three synthetic $C_4H_8O_3$ compounds with OH were then determined in individual chamber experiments. Additionally, field measurements from the isoprene-rich Southeastern United States were analyzed *vis-à-vis* the newly elucidated reaction rates and product yields. Finally, the oxidation mechanism of IEPOX and the $C_4H_8O_3$ compounds was incorporated into GEOS-Chem, a global chemical transport model, to estimate their global production and potential impact on tropospheric chemistry.

3.2 Experimental Methods

3.2.1 Synthesis

Five compounds were synthesized for use in chamber experiments: *trans-β*-IEPOX, *cis-β*-IEPOX, DHBO, 2,3-dihydroxy-2-methylpropanal (DHMP), and 2,3-dihydroxybutanal (DHBA). All compounds were characterized by 300 MHz ^{1}H NMR. Reagents were purchased from Sigma-Aldrich unless otherwise noted.

Trans-β-IEPOX was prepared from 3-methyl-2-buten-1-ol by a method identical to that used by Bates *et al.* (2014) derived from the techniques of Zhang *et al.* (2012) *cis-β*-IEPOX was prepared in a method similar to that of Bates *et al.* (2014) except that two steps of the synthetic pathway were bypassed by reducing citraconic anhydride directly to 2-methyl-2-butene-1,4-diol using diisobutylaluminum hydride (DIBAL-H), as shown in Figure 3.3. The procedure for this reduction was identical to that described for the reduction of 3-methylfuran-2(5H)-one in the original synthesis (Bates *et al.*, 2014), except that 5 equivalents of DIBAL-H were necessary to achieve the desired reaction, and the yield was reduced to 28%, slightly below the combined yield of 30% for the three steps it replaced. ^{1}H NMR spectra of *cis-* and *trans-β*-IEPOX matched previously published characterization (Bates *et al.*, 2014).

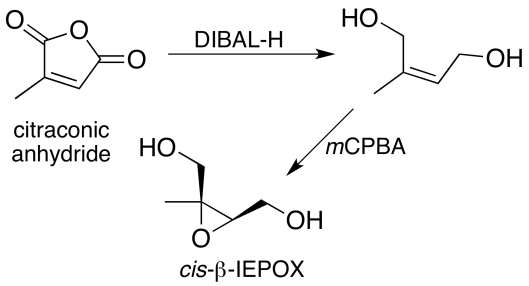

Figure 3.3: Steps in the synthesis of *cis*-β-IEPOX.

The three $C_4H_8O_3$ compounds were synthesized individually in two steps, using known procedures with slight adaptations, as shown in Figure 3.4 for the synthesis of DHBO from methyl vinyl ketone (MVK, ≥95%). DHMP and DHBA were synthesized with the same two steps, but using methacrolein (95%) and crotonaldehyde (≥99.5%, ~1:20 *cis*:*trans*) respectively as starting compounds. The starting material was first epoxidized under basic conditions (House and Ro, 1958; Payne, 1959; Wellman *et al.*, 1976) by addition to a solution of 17.5% hydrogen peroxide (H_2O_2) in water, brought to 0 °C and pH 8.5-9 by addition of NaOH. The reaction was allowed to warm to room temperature 10 min after addition; stirring continued for 2 h after addition, and during the entire reaction, pH was kept at 8.5-9 by slow addition of NaOH. After the reaction was complete, it was neutralized with HCl and the epoxide intermediate was isolated by extraction with dichloromethane (DCM), dried with Na_2SO_4, filtered, and concentrated under reduced pressure. The epoxide intermediates were then hydrolyzed (Long and Pritchard, 1956; Wang *et al.*, 2008b) in neutral aqueous solution by heating for 24 h to 65 °C (DHMP), 70 °C (DHBA), or 80 °C (DHBO). Unreacted starting material was removed by extraction with DCM; the $C_4H_8O_3$ dihydroxycarbonyl compounds remained in the aqueous phase, and were concentrated slightly under reduced pressure with minimal heating (<30 °C) and used without further purification. Where available, ^{1}H NMR spectra matched previously published characterization (Bischofberger *et al.*, 1988; Guérard-Hélaine *et al.*, 2011; Kholodar and Murkin, 2013; Wellman *et al.*, 1976).

3.2.2 Chamber experiments

Initial conditions for each of the chamber experiments conducted in this study are listed in Tables 3.1 and 3.2. The environmental chamber used for gas phase OH oxidation experiments, along with the associated techniques and instruments, has been described extensively in previous literature (Bates *et al.*, 2014; Crounse

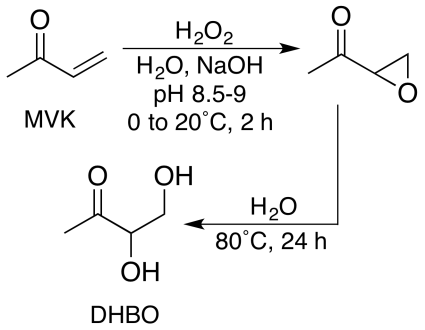

Figure 3.4: Steps in the synthesis of dihydroxybutanone (DHBO).

expt #	reactant	$[\text{reactant}]_0$ (ppbv)	$[H_2O_2]_0$ (ppbv)	$[\text{propene}]_0$ (ppbv)	$[NO]_0$ (ppbv)	reaction time (h)
1	DHBO	103.75	2.4	105	0	6.0
2	DHBO	104.61	2.9	117	580	6.0
3	DHMP	2.75	2.7	130	582	6.0
4	DHMP	5.17	2.6	166	0	6.0
5	DHMP	2.63	3.2	141	0	3.0, 3.0
6	DHBA	0.72	2.6	132	576	6.0
7	DHBA	1.60	2.6	130	576	3.0, 3.0
8	DHBA	0.34	2.9	142	0	3.0, 3.0

Table 3.1: Initial conditions for kinetic-focused chamber experiments.

et al., 2013; Lee *et al.*, 2014; St. Clair *et al.*, 2015), so only a cursory summary is provided herein, with particular detail for aspects unique to this study. Experiments were conducted in 0.85 m^3 environmental chambers made of fluorinated ethylene propylene (Teflon-FEP, DuPont) kept at 297 ± 5 K and 745 Torr, with separate chambers used for high- and low-NO experiments. The chamber was cleaned by flushing with dry air from a purge gas generator (Perkin, Model 75-52) and evacuating at least six times between experiments.

To prepare each experiment, the synthetic compound of interest was added to the chamber by flowing dry air at 20 L min^{-1} into the chamber's single sample port through a small glass vial containing ~50 μL of the target compound (pure IEPOX, or a dilute solution of $C_4H_8O_3$ in H_2O) for 30 min. For IEPOX injections, the vial was heated to 45 °C (*trans*) or 60 °C (*cis*) in a water bath. Hydrogen peroxide (50% w/w in H_2O, ~6 mg) was added by the same method for 10 min without heating, to achieve an initial mixing ratio of ~2.5 ppmv. For kinetic experiments, propene gas was added by flushing the contents of a dilute 500 cm^3 glass bulb into the chamber

expt \$	reactant	$[reactant]_0$ (ppbv)	$[H_2O_2]_0$ (ppbv)	$[NO]_0$ (ppbv)	reaction time (h)
9	*cis*-β-IEPOX	94.89	3.0	0	5.0
10	*cis*-β-IEPOX	53.28	2.8	0	8.4
11	*cis*-β-IEPOX	30.83	2.9	581	2.0, 2.0
12	*cis*-β-IEPOX	55.23	2.8	0	3.1
13	*cis*-β-IEPOX	83.82	3.2	346	1.6
14	*trans*-β-IEPOX	81.74	2.7	592	2.7
15	*trans*-β-IEPOX	131.41	3.6	0	6.2
16	*trans*-β-IEPOX	126.87	3.0	0	2.5, 3.5
17	DHBO	81.22	2.7	589	1.5
18	DHBO	74.21	2.9	0	3.0

Table 3.2: Initial conditions for product-focused chamber experiments.

with 20 L min^{-1} of dry air for 1 min. The bulb was prepared by serial dilution of propene (Sigma-Aldrich, ≥99%) to ~225 ppmv with N_2. For NO-dominated experiments, NO was added last by filling the same bulb to ~370 Torr with 1994 ± 20 ppm NO in N_2 (Matheson Gas Products) and flushing the bulb's contents into the chamber with 20 L min^{-1} of dry air for 1 min. Finally, the chamber was filled with dry air to a total volume of 850 L.

After preparing the environmental chamber, the injection port was reconnected to the sampling instruments, which measured the chamber's contents for at least 1.5 hours prior to photooxidation. Oxidation was performed using eight UV broadband lamps centered around 350 nm (Sylvania) to photolyze H_2O_2, forming OH and subsequently HO_2 by the reaction of OH with H_2O_2. Photooxidation lasted anywhere between 1.5 and 8.5 hours, and in some experiments two separate episodes of photooxidation were performed with a period of dark sampling in between, as listed in Tables 3.1 and 3.2.

Chemical species in the chamber were measured throughout the experiment through a single length of PFA tubing (6.35 mm OD, ~2 m long). A NO_x monitor (Teledyne 200 EU) and an O_3 monitor (Teledyne 400 E) sampled continuously, as did a gas chromatograph with flame ionization detection (GC-FID, Agilent 5890 II) to measure propene. IEPOX, $C_4H_8O_3$, and their oxidation products were measured with a time-of-flight chemical ionization mass spectrometer (ToF-CIMS, Tofwerk/Caltech), which has been described in detail previously (Crounse *et al.*, 2006; Paulot *et al.*, 2009a; Praske *et al.*, 2015; St. Clair *et al.*, 2010). The CIMS uses

CF_3O^- as its reagent gas, which is produced by flowing CF_3OOCF_3 in N_2 (1 ppmv) through a ^{210}Po ionizer, and provides measurements of all *m/z* between 19 and 396 at 1 Hz time resolution. CF_3O^- clusters with acids, alcohols, hydroperoxides, and other polar compounds to form ions with *m/z* equal to that of the analyte plus 85; thus, IEPOX is detected at *m/z* 203 and $C_4H_8O_3$ at *m/z* 189. All *m/z* signals are normalized to the reagent anion signal, characterized by the sum of CF_3O^-, $H_2O{\cdot}CF_3O^-$, and $H_2O_2{\cdot}CF_3O^-$, and scaled by a sensitivity factor. CIMS sensitivities were estimated from the target compound's polarizability and dipole moments, calculated using density functional theory (DFT) as described previously (Garden *et al.*, 2009; Paulot *et al.*, 2009a,b; Praske *et al.*, 2015; Su and Chesnavich, 1982). Estimated CIMS sensitivities for compounds of interest in this work are given in Table 3.7 in the Supporting Information.

Before and after photooxidation, and between photooxidation episodes in experiments 5, 7, 8, 11, and 16, the ToF-CIMS was disconnected from the chamber and connected to the outlet of a gas chromatography oven (GC-CIMS), to separate isobaric compounds in a technique described previously (Bates *et al.*, 2014; Lee *et al.*, 2014; Praske *et al.*, 2015; Teng *et al.*, 2015). 150-300 cm^3 of chamber air was cryogenically trapped on the head of a 4 m Restek RTX-1701 column for 4 – 8 min using a bath of isopropanol cooled with liquid nitrogen to -30 – -20 °C. Following the removal of the cold trap, the column temperature was ramped in the GC oven (30 °C for 0.1 min, +3 °C min^{-1} for 10 min, +10 °C min^{-1} for 7 min, hold for 3 min). Analytes were passed through the column directly into the ToF-CIMS for detection.

3.2.3 GEOS-Chem Simulations

The location and extent of production of $C_4H_8O_3$ compounds in the atmosphere was evaluated using GEOS-Chem, a global chemical transport model (Bey *et al.*, 2001). The simulations described in this study employed GEOS-Chem version 9.02 with GEOS5 meteorology and the Rosenbrock Rodas-3 solver, and were run on a 4° × 5° grid for the year 2012, following a 1.5 year spinup.

The standard isoprene mechanism included in GEOS-Chem v9.02 (Mao *et al.*, 2013) was updated to include a number of recently published results, including the separation of ISOPOOH and IEPOX isomers and revision of their reaction rates and yields (Bates *et al.*, 2014; St. Clair *et al.*, 2015); the inclusion of new deposition velocities based on recent field measurements (Nguyen *et al.*, 2015a); and revised rates and yields of photolysis and reaction with OH and O_3 for MVK (Praske *et*

al., 2015) and first- and second-generation isoprene nitrate products (Jacobs *et al.*, 2014; Jenkin *et al.*, 2012; Lee *et al.*, 2014; Müller *et al.*, 2014). Further revisions based on the results of experiments in this study, including the addition of $C_4H_8O_3$ compounds and their products, were then applied as described below and detailed in Table 3.8 in the Supporting Information.

3.2.4 Field Observations

Experimental and simulated results were compared with measurements of $C_4H_8O_3$ compounds, as well as IEPOX and other related species, taken as part of the Southern Oxidant and Aerosol Study (SOAS; SOAS2013.rutgers.edu). Observation occurred between June 1st and July 15th, 2013, at the Southeastern Aerosol Research and Characterization (SEARCH) site in Centreville, Alabama (32.903 °N, 87.250 °W). The sampling site, surrounded by predominantly deciduous forests and located >50 miles from large urban areas, provided an archetypal high-isoprene environment; isoprene comprised 82 mol% of biogenic volatile organic compounds at the site (Xu *et al.*, 2015). During the sampling period, temperatures ranged between a diurnal mean high of 28.6 °C and a mean low of 21.6 °C, while relative humidity averaged >50% during the day and >90% at night (Xu *et al.*, 2015).

The same CIMS described above was deployed at the site and operated with only minor adjustments, which have been described previously (Nguyen *et al.*, 2015a). The most significant change was the replacement of the chamber sampling line with a high-flow (2000 L min^{-1}) fluoropolymer-coated glass inlet (0.4 m long, 3.1 cm inner diameter) to minimize losses of semivolatile compounds. The CIMS was positioned atop a metal sampling tower with a measurement height of 22 m, surrounded on three sides by forest with a canopy height of 10 m, and was placed in an insulated enclosure to control the instrument's temperature.

As described above, the CIMS detected relevant compounds as clusters with CF_3O^-, adding 85 to the nominal mass. After normalization to the reagent anion signal, the CIMS counts were scaled by estimated sensitivity factors to derive mixing ratios. For any *m/z* at which a mixture of isobaric compounds was expected (*e.g.*, IEPOX and ISOPOOH at *m/z* 203, all $C_4H_8O_3$ compounds at *m/z* 189, and all $C_4H_6O_3$ compounds at *m/z* 187), an average sensitivity was computed by weighting each compound's sensitivity according to its relative abundance in a simple steady-state box model of ISOPOOH oxidation, employing the rates and product yields reported in this and previous studies (Bates *et al.*, 2014; St. Clair *et al.*, 2015).

3.3 Results and Discussion

3.3.1 $C_4H_8O_3$ + OH Rate Coefficients

Rate coefficients (k_{OH}) for the reactions of each $C_4H_8O_3$ isomer with OH were derived using data from experiments 1 – 8 (Table 3.1) and were calculated relative to that of propene ($k_{propene}$ = 2.59 × 10^{-11} cm^3 $molecule^{-1}$ s^{-1} at 298 K and 993 hPa) (Atkinson and Arey, 2003a; Atkinson *et al.*, 2006). For each experiment, a linear regression incorporating error in both dimensions (York *et al.*, 2004) was performed on the natural log of the propene mixing ratio (measured by GC-FID) versus time, giving a slope equal to $k_{propene}$ × [OH], from which [OH] was calculated. The slope derived from a similar regression performed on the $C_4H_8O_3$ mixing ratio was then divided by [OH] to provide $k_{analyte}$.

For DHBO, enough analyte could be introduced to the chamber (>100 ppbv) to provide a strong CIMS signal with high signal-to-noise, which the GC-CIMS confirmed was overwhelmingly composed of DHBO with little (<1%) isobaric impurity. This allowed the CIMS signal to be converted directly to mixing ratio, using ion-molecule collision rate-estimated sensitivity, with low risk of systematic error from background interference. The calculated mixing ratio was then used for the error-weighted linear regression described above, from which k_{DHBO} was calculated.

For DHMP and DHBA, only small amounts (0.3-5.2 ppbv) of analyte could be introduced to the chamber, and the GC-CIMS showed that isobaric impurities interfered with the raw signal at *m/z* 189. These impurities, along with background signals and low signal-to-noise, could cause appreciable systematic error in an estimation of their oxidation rates based solely on the raw CIMS signal. Therefore, the linear regressions were performed on the integrated areas of analyte peaks as measured by GC-CIMS before, after, and between photooxidation periods. This method provides less precision, because it uses far fewer data points for each linear regression, but it introduces less systematic error by isolating the CIMS signal exclusively from the analyte of interest and integrating that signal over the 4-8 min GC sample collection time.

Measured rate coefficients for the reactions of DHBO, DHMP, and DHBA with OH are reported in Table 3.3. The reported values are relative-inverse-variance-weighted averages of the individual experimentally derived coefficients. Reported uncertainties include those of the linear regressions and the propene rate coefficient, propagated through the weighted averaging. Differences between measured rate

	k_{OH} ($\times 10^{-11}$ cm^3 molec^{-1} s^{-1})		
compound	this work	MCM	SAR
DHBO	1.10 ± 0.16	1.88	1.07
DHMP	3.0 ± 0.65	3.42	2.52
DHBA	3.7 ± 0.63	7.01	3.58

Table 3.3: Rate coefficients for the reactions of DHBO, DHMP, and DHBA with OH as measured in this work, reported in MCM, and estimated by SAR.

coefficients for individual experiments performed on a given analyte did not correlate or differ appreciably with [NO].

The rate coefficients measured in these experiments are consistent with those estimated by structure-activity relationship (SAR), also reported in Table 3.3, to within one standard deviation (Kwok and Atkinson, 1995). The SAR rate coefficients for DHBO and DHBA differ by only 3% from the experimentally determined values, while that of DHMP differs by 16%. Table 3.3 also includes the rate coefficient values currently used in the Master Chemical Mechanism (MCM v3.2) (Saunders *et al.*, 2003), which show a larger deviation from experimentally determined values, but agree to within a factor of two.

3.3.2 IEPOX Product Studies

Experiments 9-16 (Table 3.2) were used to estimate product yields from the reactions of IEPOX isomers with OH. Each yield was estimated from the slope of a simple linear regression between the normalized CIMS counts at *m/z* 203 (IEPOX) and those of the observed product over the first 15-20 minutes of oxidation, during which 10% of the initial IEPOX was oxidized; in these early periods, yields were observed to be linear and the high [IEPOX]:[product] ratio minimized interference from subsequent reactions of products. The regression slope was then multiplied by the ratio between the CIMS sensitivities (Table 3.7 in the Supporting Information) of the product and IEPOX to provide fractional product yields. Yields were corrected for loss of products to reaction with OH with the methods introduced by Atkinson *et al.* (1982) Product yields calculated in high- and low-NO experiments for each isomer were not found to be statistically significantly different (using the errors of the slopes of the linear regressions); for this reason, yields from all experiments with each individual IEPOX isomer were combined with a relative-inverse-variance-weighted mean to give the values reported in Table 3.4. Additional discussion of NO dependence can be found in the mechanism description below.

	molar yields (%)		
product	*cis*-β-IEPOX	*trans*-β-IEPOX	presumed coproducts
m/z 201 ($C_5H_8O_3$)	21 ± 7	18 ± 2	HO_2
DHBO	41 ± 13	36 ± 4	CO + OH
DHMP	5 ± 2	9 ± 1	CO + OH
m/z 187 ($C_4H_6O_3$)	8 ± 2	7 ± 1	CH_2O + OH
hydroxyacetone	8 ± 1	16 ± 1	glyoxal + OH
glycolaldehyde	17 ± 5	14 ± 7	methylglyoxal + OH

Table 3.4: Experimentally determined product yields from *cis*- and *trans*-β-IEPOX + OH.

Five masses were observed to account for a near unity yield (100% for *cis*-β-IEPOX, 95% for *trans*-β-IEPOX). Reported uncertainties for all masses except *m/z* 189 include only the standard deviations of the linear regression slopes propagated through the inverse-variance averaging; additional uncertainties in CIMS sensitivities are estimated to be ±30%. Between these uncertainties and the potential for additional systematic errors (*e.g.* products rapidly lost to walls or undetectable by CIMS), carbon parity is not necessarily expected in the product yields measured herein. However, because unity yields are useful for simulations, and because the five observed product masses require little scaling to achieve that result, yields (and corresponding uncertainties) reported in Table 3.4 are scaled to achieve carbon parity. It should be noted that a number of products not observed in this study have previously been shown or proposed to form from IEPOX (Jacobs *et al.*, 2013; Saunders *et al.*, 2003); possible reasons for their lack of detection are discussed below. Should these unobserved products prove to account for a considerable yield from the reaction of IEPOX with OH, the product yields reported in this study and any conclusions drawn from them will need to be scaled accordingly.

To determine the isomeric yields of the $C_4H_8O_3$ products, the *m/z* 189 signals from GC-CIMS samples taken after and between photooxidation episodes were analyzed to determine which isomers were present. Figure 3.5 shows an example of the signals from a GC-CIMS sample taken after IEPOX oxidation, along with signals from GC-CIMS samples of the three synthetic $C_4H_8O_3$ standards. In addition to their characteristic retention times, the $C_4H_8O_3$ isomers can be distinguished by their unique ratios of coeluting fragments and alternate ion pairs (*e.g.* $C_4H_8O_3{\cdot}F^-$ at *m/z* 123), also shown in Figure 3.5. Only DHBO and DHMP were observed to form from both *cis*- and *trans*-β-IEPOX, and the integrated areas of their GC-CIMS peaks were

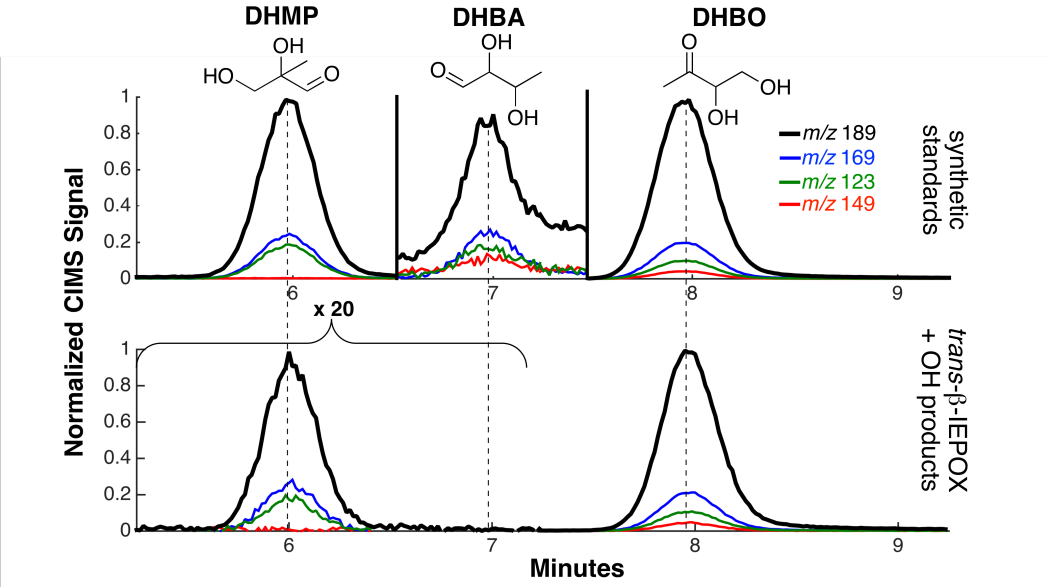

Figure 3.5: GC-CIMS chromatograms of the three synthetic $C_4H_8O_3$ standards (top) and of the products of *trans-β*-IEPOX + OH (bottom). Product signals are scaled up by 20× between 5.25 and 7.25 minutes for visibility. The products of *trans-β*-IEPOX + OH share the same retention times and coeluting masses as DHMP and DHBO.

scaled by their calculated CIMS sensitivities to provide estimated mixing ratios. A simple box model calculation was performed, incorporating IEPOX oxidation rates and the oxidation rates of the $C_4H_8O_3$ products; yields of the $C_4H_8O_3$ products were then adjusted to fit measured mixing ratios. DHBO was found to be the single highest yielding product, accounting for 43% and 36% of the products from *cis-* and *trans-β*-IEPOX respectively, while DHMP was produced in yields of 5% and 9%.

The six major products observed by CIMS in the oxidation of IEPOX by OH include hydroxyacetone, glycolaldehyde, DHBO, DHMP, and compounds observed at *m/z* 187 and 201. These products have all been observed in prior studies of IEPOX oxidation, and mechanisms to account for their formation have been previously published (Bates *et al.*, 2014; Jacobs *et al.*, 2013). An updated version of an IEPOX oxidation mechanism, originally proposed by Bates *et al.* (2014), is shown in Figure 3.6; this mechanism accounts for all six of the observed major products, and is described in detail in the following paragraph.

In the proposed mechanism, hydrogen abstraction by OH from IEPOX at carbons 1 and 4 (see numbering in Figure 3.6) can be followed immediately by reaction with O_2, forming the epoxide-retaining product at *m/z* 201 (herein labeled IEPOXO) and

generating an equivalent of HO_2. Alternatively, abstraction at carbons 1 and 4 can be followed by cleavage of the epoxide ring and an intramolecular hydrogen shift prior to O_2 addition, forming C_5 peroxy radicals. These peroxy radicals may undergo a (1,4)-H shift of the aldehydic hydrogen to the peroxy moiety, which precedent suggests will be rapid Crounse *et al.* (2012, 2013), followed by decomposition to form the $C_4H_8O_3$ dihydroxycarbonyls DHBO or DHMP along with CO and OH. Alternatively, the C_5 peroxy radicals may react with either HO_2 or NO to form alkoxy radicals, which would decompose to form either the same $C_4H_8O_3$ dihydroxycarbonyls or the hydroxyacetone and glycolaldehyde observed in these studies, along with their presumed respective coproducts of glyoxal and methylglyoxal. Yields of these C_2-C_3 products were found to increase slightly in high-NO experiments, with a minor corresponding decrease in $C_4H_8O_3$ yields, but the changes were not statistically significant. While the relative rates of isomerization and reaction with NO or HO_2 are not known for the C_5 peroxy radicals shown in Figure 3.6, the minor differences in product yields between high- and low-NO experiments suggest that formation of DHBO or DHMP may be insensitive to these rates. However, because the branching between these three reactive pathways affects radical recycling, further work should focus on determining these rates. Finally, the product at *m/z* 187 is thought to be the α-diketone 1-hydroxy-2,3-butadione (HBDO), which has also been observed as an oxidation product of MVK under low-NO conditions (Praske *et al.*, 2015). HBDO is predicted to form following hydrogen abstraction from carbon 3 of IEPOX, and would likely be accompanied by formaldehyde and OH as coproducts.

A number of products proposed in previous studies of *cis*- and *trans*-β-IEPOX do not appear in this mechanism, as they were not observed in the studies described herein. In particular, the products observed by Jacobs *et al.* (2013) at *m/z* 89, 133, and 151 ($M+H^+$) along with other C_5 compounds predicted to form in MCM (Saunders *et al.*, 2003) were not seen to form from IEPOX in these experiments. That these compounds were not observed by CIMS does not necessarily mean they were not produced; they may have been lost to chamber walls, been photolyzed, or be undetectable by CF_3O^- CIMS. However, because the observed products do achieve a result near carbon parity, unobserved products are not expected to account for a large yield, and were therefore not included in the mechanism. The formic and acetic acids observed by Bates *et al.* (2014) were also seen in the experiments conducted in the present study, but in low and highly variable yields. The organic acids were also observed in blank experiments performed without any IEPOX added to chamber, and are thought to result in part from wall reactions; furthermore, they

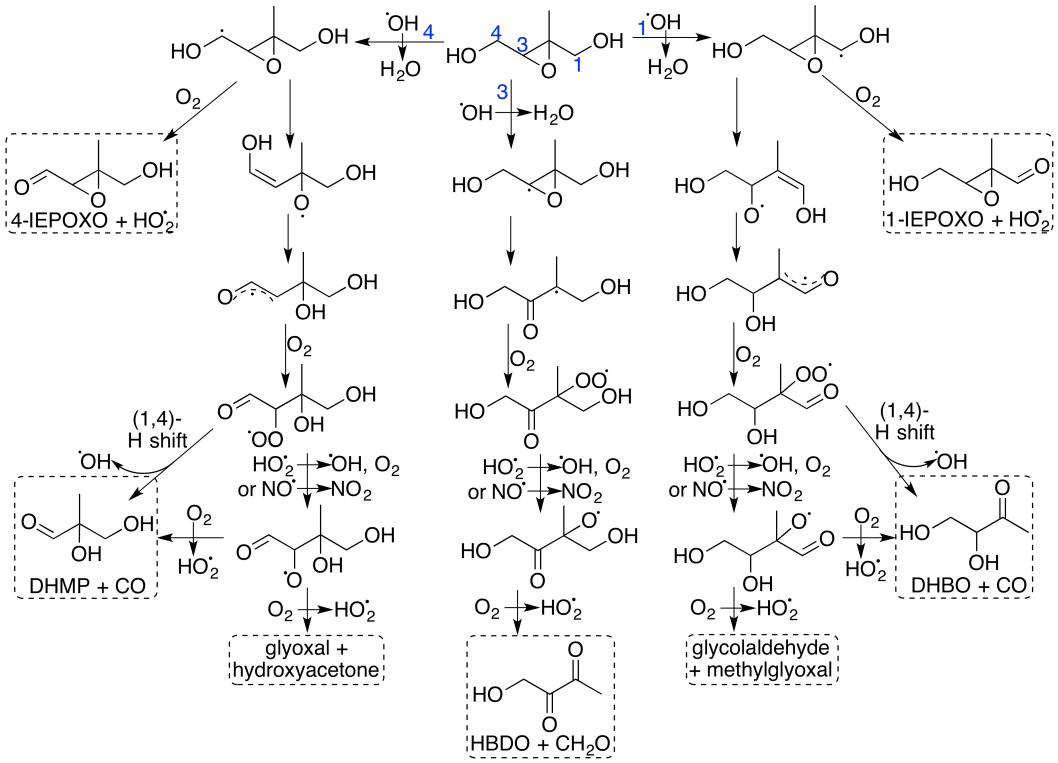

Figure 3.6: Steps in the OH-initiated oxidation of IEPOX. Stable products observed in this study are boxed. It is possible that HBDO may result from a slow (1,5)-H shift, forming HO_2 in addition to the boxed products, rather than from reaction with HO_2 or NO; similarly, though the aldehydic (1,4)-H shifts are predicted to occur quickly, the same products (CO, OH, and DHMP or DHBO) could be formed by reaction of the peroxy radicals with HO_2 or NO.

are not expected to form from IEPOX + OH by any known direct mechanism. Therefore, they were not included as products in this analysis.

Notably, five of the six major products of IEPOX + OH, accounting for ≥80% of the yield, are expected to recycle OH as a coproduct; only IEPOXO is not, though its coproduct of HO_2 still propagates the radical chain. This high recycling rate results from the intramolecular hydrogen shifts that allow for fragmentation of the IEPOX-peroxy radical before it can react with NO, HO_2, or other species present. While it is possible that the observed products could result from the reaction of IEPOX-peroxy radicals with other radical species, which would not cause such high OH recycling rates, the lack of dependence of product yields on [NO] suggests that intramolecular hydrogen shifts dominate the reaction pathways. If this is true, the first generation of IEPOX oxidation should not be considered oxidant-consuming, and may contribute to sustained high OH concentrations over remote forests.

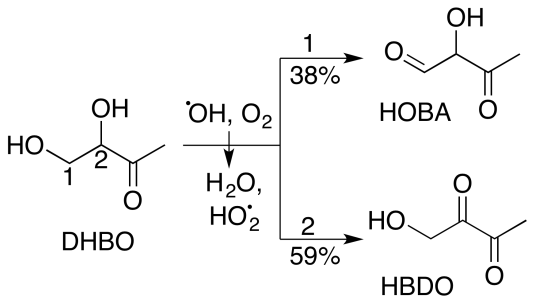

Figure 3.7: Anticipated products of DHBO + OH. Yields are calculated by SAR.

3.3.3 $C_4H_8O_3$ Oxidation Product Studies

Since DHBO was observed to be the highest yielding product from IEPOX + OH, and because it could be introduced in high quantity and purity to the chamber, experiments 17-18 were performed to examine the products of its oxidation by OH. The two experiments – one with and one without NO – were executed and analyzed in a manner identical to that of the IEPOX product yield experiments.

Because the α-hydroxy hydrogens of DHBO are expected to be most labile, the anticipated mechanism of DHBO + OH would involve H abstraction at carbons 1 or 2 (see numbering in Figure 3.7), followed by addition of O_2 and loss of HO_2 to convert one of the alcohols into a carbonyl group, as illustrated in Figure 3.7. The resulting $C_4H_6O_3$ compound would be detected by CIMS at *m/z* 187. By SAR (Kwok and Atkinson, 1995), abstraction at carbon 2 is estimated to account for 59% of OH reactivity, which would form the α-diketone HBDO, itself a direct product of IEPOX + OH as discussed above. Abstraction at carbon 1, accounting for 38% of OH reactivity, would form 2-hydroxy-3-oxobutanal (HOBA). CIMS sensitivities to these compounds, along with the analogous 2-hydroxy-2-methylpropanedial (HMPD) that would form from α-hydroxy hydrogen abstraction of DHMP, were estimated by the method described above, and are shown in Table 3.7 in the Supporting Information.

As expected, in experiments 17 and 18, compounds detected by CIMS at *m/z* 187 were the only major products observed from DHBO + OH. The combined yield of these compounds was estimated by taking a simple linear regression between the normalized CIMS counts at *m/z* 189 and *m/z* 187 over the first 15-30 minutes of oxidation, during which 5% of the DHBO was consumed. The resulting slope was scaled by a ratio of the compounds' estimated CIMS sensitivities; the CIMS sensitivity to the *m/z* 187 products was calculated as an average of the two products predicted above by SAR, weighted by their expected yields. Computed yields from

the two experiments were then averaged in a relative-inverse-variance-weighted mean to give a combined $C_4H_6O_3$ yield of (96 ±14)%, which is statistically indistinguishable from both the SAR results and a unity yield. Unfortunately, the $C_4H_6O_3$ products did not separate reliably on the GC-CIMS column, and a lack of synthetic standards prevented their identification, but the agreement of the combined yield with the SAR predictions suggests that the isomeric breakdown from SAR provides a reasonable estimate of individual HBDO and HOBA yields from DHBO.

Although the chain of gas phase IEPOX oxidation products could not be extended further in these experiments, some degree of conjecture on subsequent reactions may provide a useful framework for chemical models such as MCM and GEOS-Chem. A speculative oxidation mechanism, extending from the $C_4H_8O_3$ products of IEPOX to molecules already appearing in GEOS-Chem, can be found in Figure 3.8. This mechanism was compiled from SAR calculations, reactions already in the MCM, and analogy to previous work on similar pathways.

Due to the speculative nature of the proposed mechanism in Figure 3.8, it will only be considered briefly here. As discussed above, DHBO reacts with OH to form HBDO and HOBA. These two $C_4H_6O_3$ compounds can then react with OH as well, with rate coefficients estimated by SAR in Table 3.9 in the Supporting Information. HOBA + OH is expected to form an acylperoxy radical, which would then decompose or react with NO or HO_2 to form methylglyoxal and CO (perhaps through a peracid intermediate when reacting with HO_2). HBDO would most likely photolyze, as has been previously reported for α-diketones (Bouzidi *et al.*, 2014). Praske *et al.* (2015) measured a "loosely constrained" photolysis rate for HBDO of 1×10^{-5} s^{-1} (for laboratory J_{NO_2} of 2.5×10^{-3} s^{-1}). Photolysis of HBDO and subsequent reaction with O_2 would produce a peroxyacetyl radical (denoted MCO_3 in GEOS-Chem) and a hydroxyperacetyl radical, the latter of which is predicted in MCM to react with other radical species and fragment to form CO_2 and CH_2O. Both HOBA and HBDO could also react with OH to form a C_4 tricarbonyl, which would then rapidly photolyze or react with OH; the most likely products of this fragmentation would be CO and the peroxyacetyl radical. DHMP, the other $C_4H_8O_3$ product of IEPOX, is also expected to react with OH, forming either 2-hydroxy-2-methylpropanedial (HMPD) or a DHMP-acylperoxy radical. HMPD – the third $C_4H_6O_3$ compound in this mechanism, along with HBDO and HOBA – is itself expected to react with OH, with a rate coefficient estimated by SAR (Table 3.9 in the Supporting Information), eventually fragmenting to form methylglyoxal. The

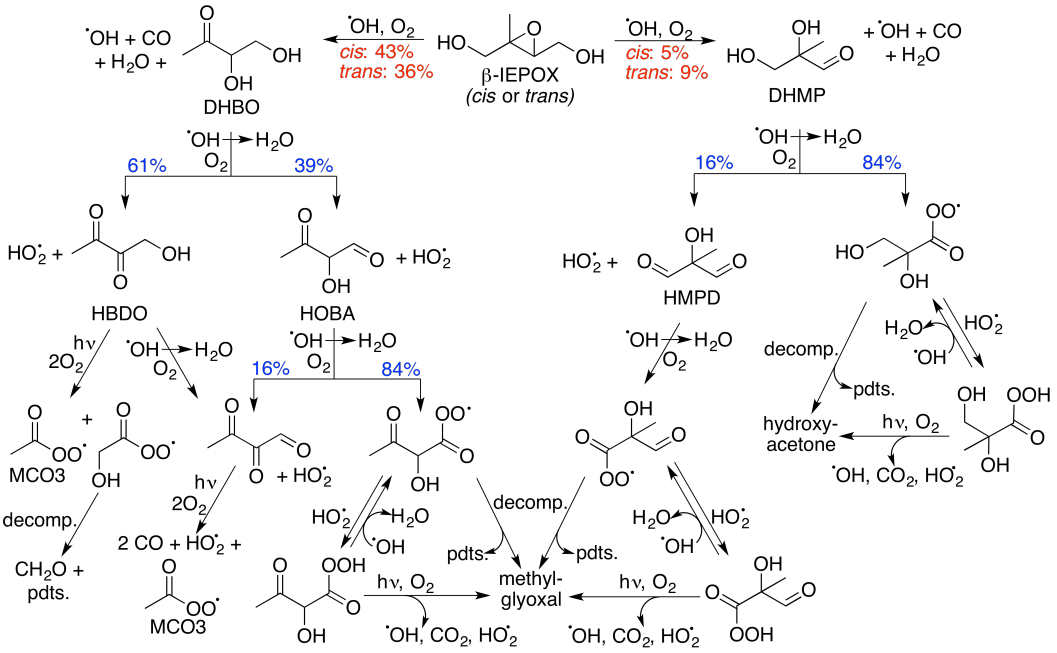

Figure 3.8: Anticipated steps in the OH-initiated of oxidation of DHBO and DHMP. Product yields in blue are calculated by SAR; those in red are measured in the present study. Reaction pathways of acylperoxy radicals labeled "decomp." may occur by a number of pathways (leading to various differing coproducts, labeled "pdts.") including: internal H shifts, producing OH and CO_2; fragmentation prior to O_2 addition to the alkyl radical, followed by reaction with O_2 to produce CO and HO_2; reaction with NO and O_2, producing NO_2, CO_2, and HO_2; reaction with RO_2 and O_2, producing RO, CO_2, and HO_2; or reaction with HO_2 and O_2, producing OH, O_2, CO_2, and HO_2. Stable products of reactions between organic radicals and NO_x (*e.g.*, peroxyacyl nitrates), while possible, are not shown in this mechanism.

DHMP-acylperoxy radical can decompose or react with NO or HO_2, eventually fragmenting to form hydroxyacetone.

A simplification of the mechanism in Figure 3.8 was incorporated into GEOS-Chem using the reactions in Table 3.8 in the Supporting Information for this study. While the mechanism may offer reasonable assumptions for chemical models of IEPOX oxidation, it should be stressed that the majority of reactions shown in Figure 3.8 are speculative. Further work is required to connect the observed first- and second-generation gas phase products of IEPOX + OH to the smaller compounds already incorporated into models, and to better constrain the radical recycling in these pathways.

3.3.4 GEOS-Chem Simulations

GEOS-Chem simulations were used to estimate the global effects of the chemistry explored in this work and to investigate where in the atmosphere it occurs. To the updated GEOS-Chem isoprene mechanism described above were added a number of new chemical species, including the two $C_4H_8O_3$ compounds observed to form from IEPOX + OH, the three $C_4H_6O_3$ isomers they produce, and the $C_5H_8O_3$ product of IEPOX + OH. Chemical reactions added to the GEOS-Chem model can be found in Table 3.8 in the Supporting Information. Wherever possible, these new reactions incorporated the measured rates and yields found in this work; for reactions lacking experimental verification, rates were estimated by SAR. Temperature dependences of rate coefficients were extrapolated from those of similar compounds existing in the GEOS-Chem mechanism. An additional simulation was run in which HBDO was allowed to photolyze, using the loosely constrained rate suggested by Praske *et al.* (2015); results unique to this simulation, which differs appreciably from the primary simulation only in its modeled concentrations of $C_4H_6O_3$ compounds, are shown in Figure 3.11 in the Supporting Information.

Simulated annual average mixing ratios of IEPOX, IEPOXO, $C_4H_8O_3$ compounds, and $C_4H_6O_3$ compounds in the lowest 1 km of the atmosphere are shown in Figure 3.9. As expected, simulated concentrations of IEPOX and its products are highly correlated. Maximum mixing ratios of $C_4H_8O_3$ compounds are seen in remote and heavily forested equatorial regions, including the Amazon and Congo Basins; in the latter, the $C_4H_8O_3$ mixing ratio reaches an annually averaged peak of 420 pptv in the lowest 1 km of the atmosphere. Mixing ratios of $C_4H_6O_3$ and IEPOXO are collocated with those of $C_4H_8O_3$, reaching maxima of 460 pptv and 70 pptv respectively in the Congo Basin. Seasonal average mixing ratios can be found in Figure 3.12 in the Supporting Information; as expected, simulated concentrations of IEPOX and its products increase over forests during the summer months. The inclusion of the $C_4H_8O_3$ and $C_4H_6O_3$ compounds and their coproducts and products in these simulations caused only minor (<3%) changes in tropospheric oxidant levels, as shown in Figure 3.13 in the Supporting Information, but the oxidant recycling in these and later steps of the mechanism is still largely unknown.

In addition to mixing ratios, GEOS-Chem can provide estimates of total annual production of selected compounds, which are listed in Table 3.5. From isoprene emissions of 515 Tg y^{-1}, the simulations performed here estimate that 352 Tg y^{-1} of ISOPOOH are produced, which go on to form 230 Tg y^{-1} of IEPOX. Further gen-

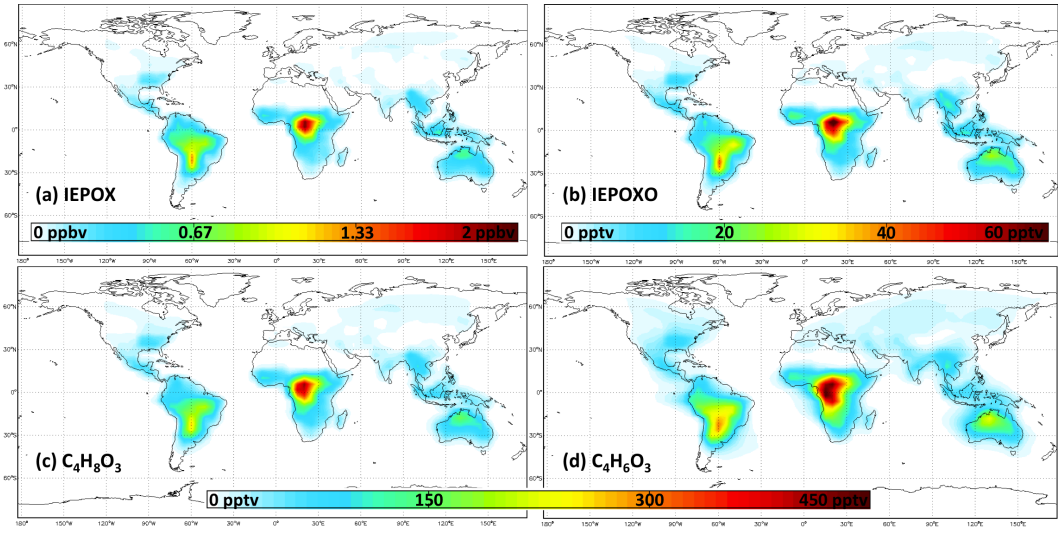

Figure 3.9: Annual average mixing ratios of IEPOX, IEPOXO, $C_4H_8O_3$ dihydroxycarbonyl compounds, and their $C_4H_6O_3$ products in the lowest 1 km of the atmosphere, as simulated using GEOS-Chem.

erations of oxidation from IEPOX then produce 54 Tg y^{-1} of $C_4H_8O_3$ compounds (84% DHBO, 16% DHMP), 51 Tg y^{-1} of $C_4H_6O_3$ compounds (49% HBDO, 31% HOBA, 20% HMPA), and 25 Tg y^{-1} of IEPOXO. Of the $C_4H_8O_3$ dihydroxycarbonyl compounds produced, 7% are estimated to be lost to deposition using the rates estimated by Nguyen *et al.* (2015a) and the rest to oxidation by OH. For all species investigated, approximately 80% of production occurs in the tropics (24 °S – 24 °N). While the low spatial resolution and simplification of certain reactions and processes in these GEOS-Chem simulations necessarily render estimated production and mixing ratios imprecise, the results shown here indicate that an appreciable fraction of isoprene reacts to form $C_4H_8O_3$ and $C_4H_6O_3$ compounds, and therefore imply that the subsequent chemistry of these compounds will impact local tropospheric oxidant and carbon budgets.

3.3.5 Field Observations

To evaluate the new IEPOX oxidation mechanism in an isoprene-rich environment, CIMS measurements obtained in Alabama during the summer of 2013 as part of the SOAS field campaign were analyzed. Figure 3.10 shows CIMS measurements at *m/z* 203 (ISOPOOH/IEPOX·CF_3O^-), *m/z* 189 ($C_4H_8O_3$·CF_3O^-), and *m/z* 187 ($C_4H_6O_3$·CF_3O^- or $C_5H_8O_2$·CF_3O^-) for a representative two weeks during the summer. While the CIMS was able to detect IEPOXO at *m/z* 201 ($C_5H_8O_3$·CF_3O^-) as well, isobaric interferences from isoprene hydroperoxy aldehydes, formed by a

	production (Tg y^{-1})					
compound(s)	total	northern hemisphere	southern hemisphere	tropics	northern extratropics	southern extratropics
ISOPOOH	351.8	147.9	203.9	295.7	30.7	25.5
IEPOX	230.0	100.1	129.9	187.6	23.4	19.1
$C_4H_8O_3$	53.5	23.0	30.5	41.9	6.1	5.5
$C_4H_6O_3$	51.4	22.0	29.5	39.7	6.0	5.7
IEPOXO	25.3	10.9	14.4	19.8	2.9	2.6

Table 3.5: Annual global production of compounds in the low-NO oxidation mechanism of isoprene, as simulated with GEOS-Chem.

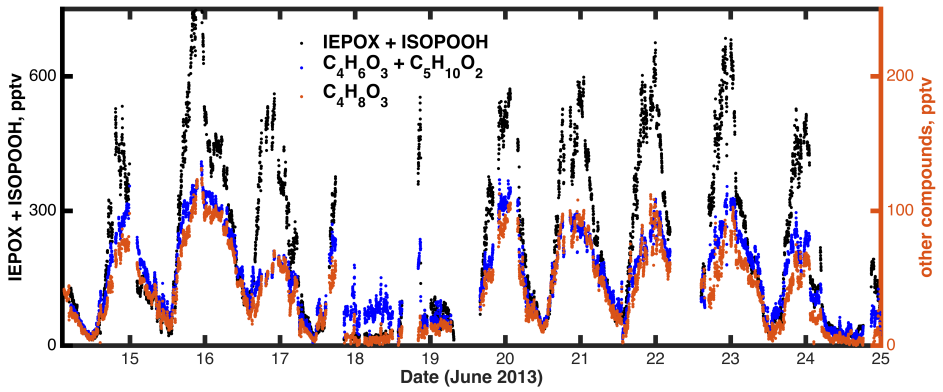

Figure 3.10: CIMS measurements of selected compounds in the low-NO oxidation pathway of isoprene during a section of the SOAS field campaign in Centreville, Alabama.

different oxidation mechanism, prevented the detailed analysis of IEPOXO in these field measurements (Crounse *et al.*, 2011).

All three masses displayed in Figure 3.10 show appreciable atmospheric loading throughout the summer, peaking at daytime averages of ~600 pptv of ISOPOOH + IEPOX and ~100 pptv apiece of $C_4H_8O_3$ and $C_4H_6O_3$. Furthermore, signals at the three masses have a remarkably high correlation, indicative either of coemission from a single source or of coproduction as part of the same mechanism. The results of both simple and error-weighted (York *et al.*, 2004) linear regressions between product masses and those of their putative progenitors are shown in Table 3.6. $C_4H_8O_3$ and $C_4H_6O_3$ show high correlations with ISOPOOH + IEPOX (r^2 = 0.83 and 0.81 respectively) and no indication of separate slopes from interfering isobaric species. While methylbutene diols ($C_5H_8O_2$) produced from isoprene nitrates might be expected to interfere with the signal of isobaric $C_4H_6O_3$ compounds, the low

	ratios			goodness of fit	
ratio	error-weighted regression	simple linear regression	GEOS-Chem	σ_{slope}, error-weighted regression	r^2, simple linear regression
$C_4H_8O_3/C_5H_{10}O_3$	0.16	0.15	0.18	0.006	0.83
$C_4H_6O_3/C_5H_{10}O_3$	0.16	0.16	0.121	0.006	0.81
$C_4H_6O_3/C_4H_8O_3$	1.04	1.00	1.20	0.006	0.92

Table 3.6: Ratios between concentrations of compounds in the low-NO oxidation mechanism of isoprene, as measured during SOAS and simulated using GEOS-Chem.

correlation between isoprene nitrates and *m/z* 187 (r^2 = 0.42; see Figure 3.14 in the Supporting Information) suggests that $C_4H_6O_3$ dominates the *m/z* 187 signal. $C_4H_8O_3$ and $C_4H_6O_3$ also correlate exceptionally well with each other (r^2 = 0.92), as shown in Figure 3.15 in the Supporting Information. That the slope between the two compounds' concentrations is so nearly unity may simply be an impressive coincidence, considering that it conflates both their respective yields and their oxidation and photolysis rates, which are unlikely to be equal.

To further explore the relationships between the low-NO products of isoprene oxidation, the product ratios measured during SOAS were compared to the results of the GEOS-Chem simulations discussed above. The relevant GEOS-Chem results were selected as the average summertime (June 21 – September 22, 2012) mixing ratios in the lowest 1 km of the atmosphere over the grid box containing the Alabama field site; the relevant ratios of these concentrations are listed in column five of Table 3.6. The newly implemented GEOS-Chem mechanism effectively captures the ratios of $C_4H_8O_3$ and $C_4H_6O_3$ to ISOPOOH + IEPOX, overpredicting them by only 13% and 31% respectively. The GEOS-Chem simulation including HBDO photolysis underpredicts the ratio of $C_4H_6O_3$ to ISOPOOH + IEPOX by 56%; however, because of the isobaric interference of $C_5H_8O_2$ with $C_4H_6O_3$ in the SOAS data, this underprediction may not be as severe as it seems. The general agreement between GEOS-Chem results and field observations implies that, despite the gaps remaining in our understanding of the low-NO gas phase oxidation pathways of isoprene, the mechanism presented herein can adequately represent the $C_4H_8O_3$ and $C_4H_6O_3$ generations of products.

3.4 Conclusions

Despite the importance of IEPOX as a product of isoprene oxidation, as evidenced by its simulated annual production of 230 Tg y^{-1} and observed daytime mixing ratios of ~600 pptv, its fate in the atmosphere remains poorly constrained. Many studies have focused on its reactive partitioning into particles, identifying a number of factors influencing its rate of uptake, but when active sites on particles are low in isoprene-rich environments, IEPOX loss is likely dominated by reaction with OH in the gas phase, with deposition and particle uptake contributing to a lesser extent. While the rates of reactions between OH and IEPOX isomers have been described previously, disagreement persists as to the reactions' products, and the lack of authentic standards in prior product studies precluded the differentiation of isobaric species.

This study has significantly reduced uncertainties in the gas phase oxidation mechanism of IEPOX, both in the first and second generations. Using synthetic standards, DHBO was conclusively identified as the major product of both *cis*- and *trans*-β-IEPOX + OH, while the isobaric DHMP was found to be a relatively minor coproduct. Both DHBO and DHMP were then reacted with OH, along with a third $C_4H_8O_3$ isomer, to examine their rates of oxidation, and the products of DHBO + OH were discussed. Finally, GEOS-Chem modeling and field observations revealed that the $C_4H_8O_3$ isomers and their $C_4H_6O_3$ products contribute substantially to total concentrations of volatile organic compounds (VOCs) in isoprene-rich, low-NO environments.

While this study marks the first laboratory investigation of $C_4H_8O_3$ dihydroxycarbonyls in the gas phase, and their first conclusive isomeric identification from atmospheric precursors, it should not be the last; considering their noted importance as oxidation products of isoprene, continued study of the $C_4H_8O_3$ isomers is warranted to further elucidate their oxidation pathways and determine whether they or their products contribute to SOA creation, tropospheric oxidant budgets, or the formation of other important VOCs. Deposition rates of the $C_4H_8O_3$ and $C_4H_6O_3$ compounds have already been measured at SOAS (Nguyen *et al.*, 2015a), but additional observation of $C_4H_8O_3$ dihydroxycarbonyls in the ambient atmosphere will help to constrain the fate of IEPOX and quantify the relative rates of its reaction with OH versus uptake to particles. Finally, incorporation of the $C_4H_8O_3$ compounds, their products, and the updated mechanisms proposed in this study into chemical models such as MCM and GEOS-Chem may improve the models' ability

to replicate VOC and oxidant budgets in isoprene-rich environments, particularly once further work has been done to solidify the $C_4H_8O_3$ compounds' complete oxidative mechanisms.

3.5 Supporting Information

compound	dipole (D)	polarizability (Å^3)	sensitivity
trans-β-IEPOX	2.47	8.98	0.371
cis-β-IEPOX	1.00	9.01	0.231
IEPOXO	1.93	8.57	0.303
DHBO	2.35	7.49	0.358
DHMP	2.09	7.52	0.331
DHBA	2.22	8.69	0.353
HBDO	2.14	7.22	0.335
HMPD	1.00	8.35	0.233
HOBA	1.08	7.27	0.228

Table 3.7: Estimated CIMS sensitivities (in normalized counts per ppbv in the inlet flow), along with their constituent parameters, for species relevant to this study.

The dipole and polarizability of the molecules are calculated with use of density functional theory at the B3LYP level, with the basis sets: 6-31G(d), 6-31+G(d) or ccpVTZ. The sensitivity is related to the relative collision rate and depends mostly on the dipole moment of the molecule colliding with the ion. The dipole moments listed in Table 3.7 are the dipole moment averaged over the possible conformers with a Boltzmann abundance larger than 0.1%. The polarizability is similar for different conformers, and the collision rate has a weak dependence on the polarizability, and is thus only calculated for the lowest energy conformer. The calculated sensitivities are estimated to have an error of less than 10%.

reactants	products	rate coefficient $k = A \times e^{r/T}$		reference
		A	r	
$RIO_2 + HO_2$	0.629×(1,2)-ISOPOOH + 0.272×(4,3)-ISOPOOH + 0.037×δ-ISOPOOH + 0.063×(OH + HO_2 + CH_2O) + 0.025×MACR + 0.038×MVK	2.06×10^{-13}	1300	1
(1,2)-ISOPOOH + OH	0.75×RIO_2 + 0.25×HC_5OO + 0.125×(OH + HO_2)	6.13×10^{-12}	200	1
(1,2)-ISOPOOH + OH	0.85×OH + 0.15×HC_5OO + 0.578×*trans*-β-IEPOX + 0.272×*cis*-β-IEPOX	1.70×10^{-11}	390	1
(4,3)-ISOPOOH + OH	0.48×RIO_2 + 0.52×HC_5OO + 0.26×(OH + HO_2)	4.14×10^{-12}	200	1
(4,3)-ISOPOOH + OH	OH + 0.68×*trans*-β-IEPOX + 0.32×*cis*-β-IEPOX	2.97×10^{-11}	390	1
δ-ISOPOOH + OH	0.25×RIO_2 + 0.75×HC_5OO + 0.375×(OH + HO_2)	5.11×10^{-12}	200	1
δ-ISOPOOH + OH	0.5×(OH + δ-IEPOX + HC_5OO)	2.92×10^{-11}	390	1
trans-β-IEPOX + OH	0.83×OH + 0.45×CO + 0.36×DHBO + 0.09×DHMP + 0.08×(HBDO + CH_2O) + 0.17×(IEPOXO + HO_2) + 0.16×(HAC + GLYX) + 0.14×(GLYC + MGLY)	3.73×10^{-11}	-400	2
cis-β-IEPOX + OH	0.8×OH + 0.48×CO + 0.43×DHBO + 0.05×DHMP + 0.08×(HBDO + CH_2O) + 0.2×(IEPOXO + HO_2) + 0.08×(HAC + GLYX) + 0.16×(GLYC + MGLY)	5.79×10^{-11}	-400	2
δ-IEPOX + OH	0.6×IEPOXDOO + 0.4×(IEPOXO + HO_2)	3.20×10^{-11}	-400	2, 3, 4
IEPOXO + OH	OH + 1.5×CO + 0.5×(CH_2O + MGLY + HAC)	9.85×10^{-12}	410	3, 4, 5
IEPOXDOO + HO_2	HAC + GLYC + HO_2 + OH	2.06×10^{-13}	1300	3, 4
IEPOXDOO + NO	HAC + GLYC + HO_2 + NO_2	2.70×10^{-12}	350	3, 4
DHBO + OH	HO_2 + 0.609×HBDO + 0.391×HOBA	8.70×10^{-12}	70	this work
DHMP + OH	0.838×(HAC + CO_2 + OH) + 0.162×(HMPD + HO_2)	7.49×10^{-12}	410	this work
DHBA + OH	1.528×CO_2 + 0.764×(ALD_2 + OH) + 0.236×(HOBA + HO_2)	9.38×10^{-12}	410	this work
HBDO + OH	2×CO + MCO_3 + HO_2	2.13×10^{-12}	70	4, 5
HMPD + OH	MGLY + CO_2 + OH	1.06×10^{-11}	410	4, 5
HOBA + OH	MGLY + CO_2 + OH	6.27×10^{-12}	410	4, 5

Table 3.8: Reactions in the low-NO isoprene oxidation pathway edited or added to GEOS-Chem for the simulations performed in this study. Standard GEOS-Chem notation is used for product abbreviations. References listed include [1](St. Clair *et al.*, 2015), [2](Bates *et al.*, 2014), [3](Jacobs *et al.*, 2013), [4](Saunders *et al.*, 2003), and [5](Kwok and Atkinson, 1995).

	k_{OH} (10^{-11} cm^3 molec^{-1} s^{-1})	
compound	MCM	SAR
HBDO	0.27	0.27
HMPD	13.2	4.18
HOBA	2.45	2.48

Table 3.9: Rate coefficients for the reactions of $C_4H_6O_3$ hydroxydicarbonyl compounds with OH, as used in the Master Chemical Mechanism v3.2 (MCM) (Saunders *et al.*, 2003) and calculated by structure-activity relationship (SAR) (Kwok and Atkinson, 1995).

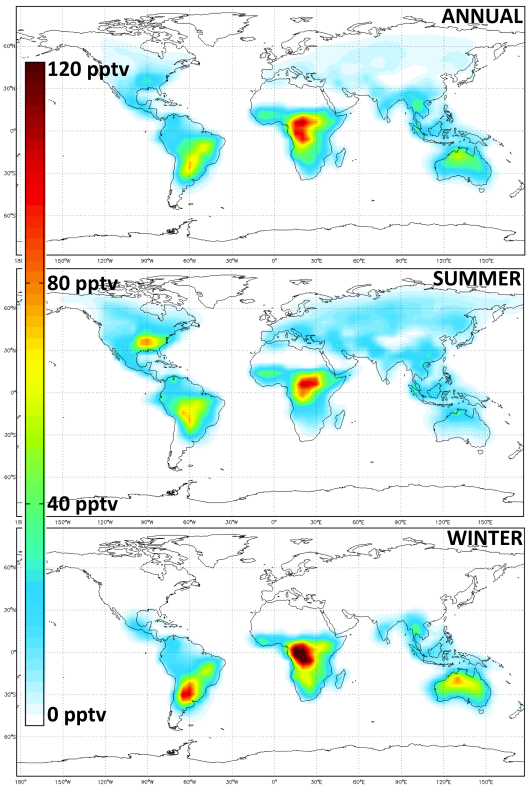

Figure 3.11: Annual and seasonal average mixing ratios of $C_4H_6O_3$ dihydroxycarbonyl compounds in the lowest 1 km of the atmosphere, as simulated using GEOS-Chem and including photolysis of HBDO.

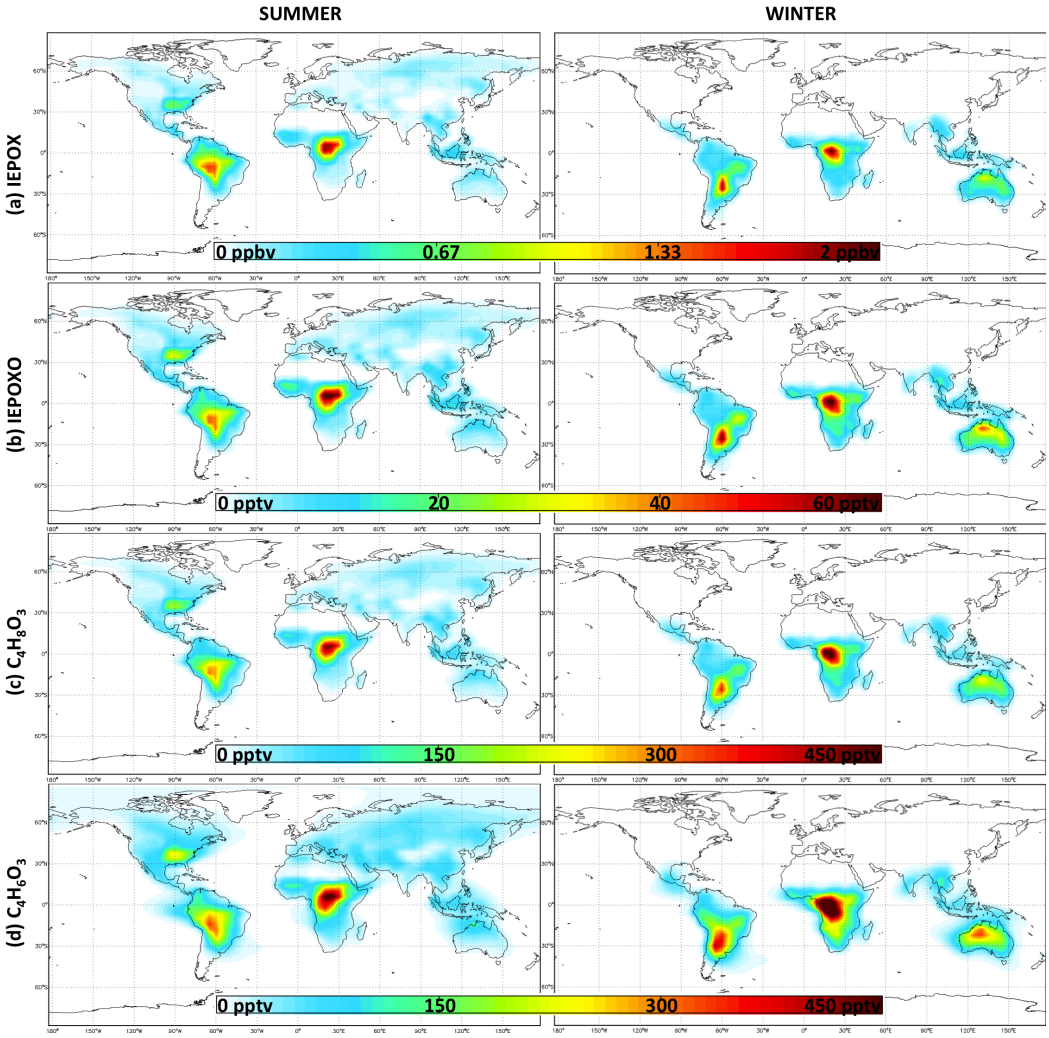

Figure 3.12: Seasonal average mixing ratios of IEPOX, IEPOXO, $C_4H_8O_3$ dihydroxycarbonyl compounds, and their $C_4H_6O_3$ products in the lowest 1 km of the atmosphere, as simulated using GEOS-Chem.

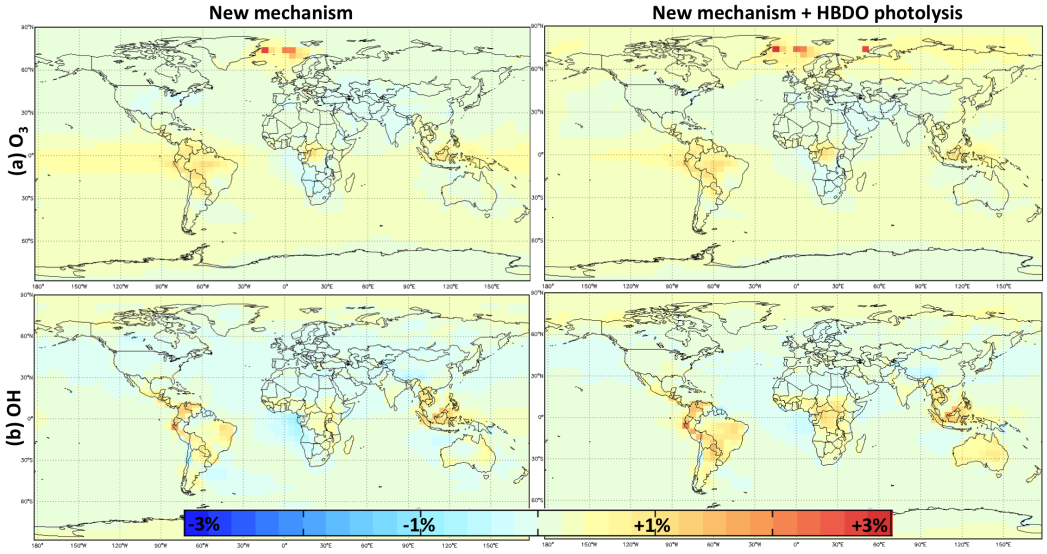

Figure 3.13: Percent changes in annual average OH and O_3 mixing ratios in the lowest 1 km of the atmosphere caused by the inclusion of the $C_4H_8O_3$ and $C_4H_6O_3$ compounds and their coproducts and products, as compared with a mechanism using the products of IEPOX + OH originally included in GEOS-Chem v.9-02 (Paulot *et al.*, 2009b).

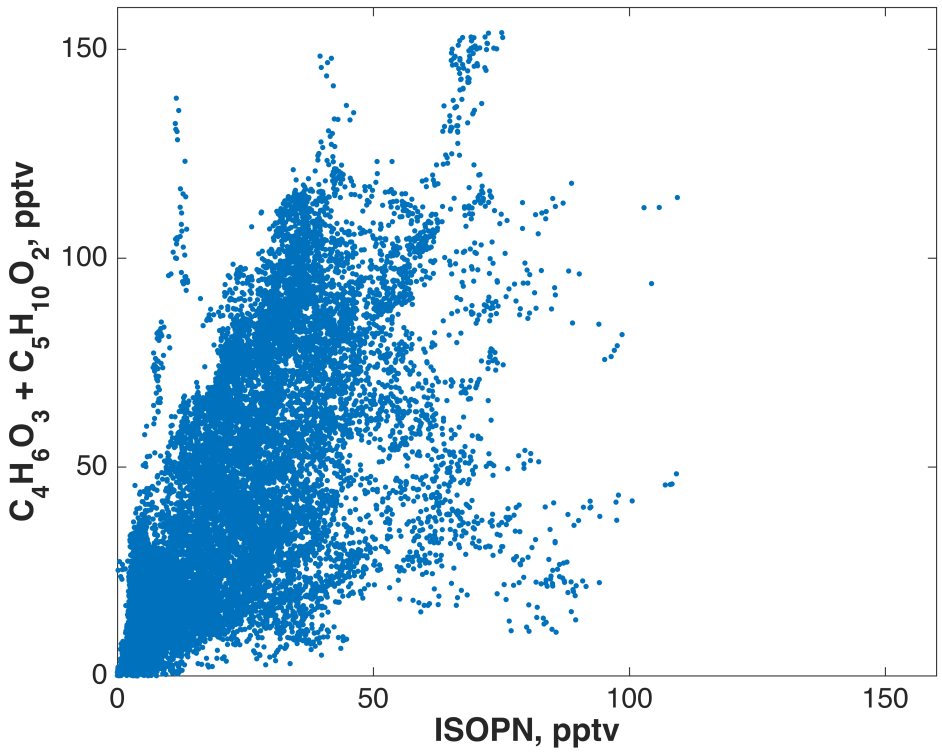

Figure 3.14: Correlation between isoprene nitrates and $C_4H_6O_3$ + $C_5H_{10}O_2$ during the entire SOAS campaign.

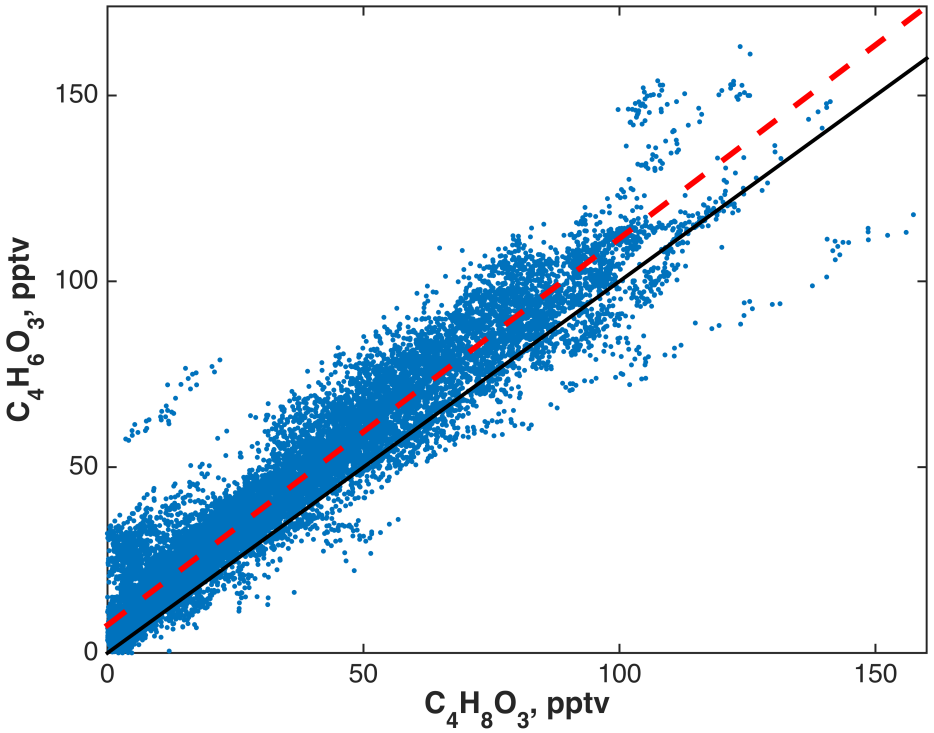

Figure 3.15: Correlation between $C_4H_8O_3$ and $C_4H_6O_3$ during the entire SOAS campaign, overlaid with a line of best fit (red, dashed; r^2 = 0.92) and a 1:1 line (black, solid).